

The experimental observation of quantum Hall effect of $l = 3$ chiral quasiparticles in trilayer graphene

Liyuan Zhang^{1,2,3}, Yan Zhang³, Jorge Camacho¹, Maxim Khodas^{1,4} and Igor Zaliznyak^{1*}

The linear dispersion of the low-energy electronic structure of monolayer graphene supports chiral quasiparticles that obey the relativistic Dirac equation and have a Berry phase of π (refs 1,2). In bilayer graphene³, the shape of the energy bands is quadratic, and its quasiparticles have a chiral degree, $l = 2$, and a Berry phase of 2π . These characteristics are usually determined from quantum Hall effect (QHE) measurements in which the Berry phase causes shifts in Shubnikov-de Haas (SdH) resistance oscillations. The QHE in graphene also exhibits an unconventional sequence of plateaux of Hall conductivity, σ_{xy} , with quantized steps of $4e^2/h$, except for the first plateau, where it is governed by the Berry phase. Here, we report magnetotransport measurements in ABC-stacked trilayer graphene, and their variation with carrier density, magnetic field and temperature. Our results provide the first evidence of the presence of $l = 3$ chiral quasiparticles with cubic dispersion, predicted to occur in ABC-stacked trilayer graphene^{4–12}. The SdH oscillations we observe suggest Landau levels with four-fold degeneracy, a Berry phase of 3π , and the marked increase of cyclotron mass near charge neutrality. We also observe the predicted unconventional sequence of QHE plateaux, $\sigma_{xy} = \pm 6e^2/h, \pm 10e^2/h$, and so on.

Despite significant interest in studying layered graphene systems with more than two layers, experimental progress has been limited^{13–18}. Low-energy electronic properties depend crucially on the stacking order of graphene layers^{4–12,18}, and therefore such studies require samples with a well-defined stacking sequence. In a bilayer, two honeycomb nets of carbon atoms are positioned with half of the atoms of the top layer (B) right above the atoms of the bottom layer (A) and the other half at the centres of the hexagonal voids in the bottom layer. The third carbon net in a trilayer can either be placed with its atoms above the atoms of the bottom layer A, as in the Bernal structure of crystalline graphite¹⁹, or with its voids above the lined-up atom pairs in layers A and B, thus breaking the reflection symmetry (Fig. 1a). The latter, ABC stacking, is found in the metastable rhombohedral modification of graphite¹⁹.

The electronic structure of graphene multilayers is derived from the hybridization of monolayer states through interlayer hopping. Its main features are captured already by only considering hopping between the nearest-neighbour carbons, which are stacked above each other in two adjacent layers, $\gamma_1 \sim 0.1\gamma_0$, as shown in Fig. 1a ($\gamma_0 \approx 3.16$ eV is the intralayer hopping, in bulk graphite $\gamma_1 \approx 0.4$ eV, and there are also further-neighbour hoppings, γ_2 – γ_5 , which are not shown)^{9–12}. In a bilayer, low-energy electronic states retain

the chiral character but have flatter, quadratic dispersion. The effective Hamiltonian is the nonlinear generalization of Dirac–Weyl quasiparticles of the monolayer,

$$\hat{H}_l = v_l \xi^l \begin{pmatrix} 0 & (\hat{\pi}^+)^l \\ \hat{\pi}^l & 0 \end{pmatrix} = v_l \xi^l p^l (\hat{\sigma}_x \cos(l\xi\varphi_p) + \hat{\sigma}_y \sin(l\xi\varphi_p))$$

with $l = 2$. Here, $v_l = v^l/\gamma_1^{l-1}$, where $v = \gamma_0(a\sqrt{3}/2\hbar) \approx 10^6$ m s⁻¹ is the velocity of linear dispersion in the monolayer, $\mathbf{p} = (p_x, p_y) = p(\cos\varphi_p, \sin\varphi_p)$ is the 2D momentum, $\pi = p_x + i\xi p_y$, $\hat{\sigma}_{x,y}$ are the pseudo-spin Pauli matrices, and $\xi = \pm 1$ is a valley index. There are two low-energy valleys with opposite chirality. For our purposes they can be considered non-interacting and yielding only a two-fold degeneracy of all states; together with the two-fold electron spin degeneracy this gives a factor of four in the Hall conductivity quantization, $4e^2/h$. The wave functions of such degree- l chiral quasiparticles acquire a Berry phase of πl on an adiabatic propagation along a closed orbit. In a bilayer, this results in $l = 2, 2\pi$ chiral quasiparticles and an unusual integer quantum Hall effect sequence with a double step, $\Delta\sigma_{xy} = 8e^2/h$, between the hole and electron gases across the $N = 0$ Landau level (LL) observed in experiment³.

The low-energy band structure of the ABA stacked graphene trilayer consists of superimposed linear and quadratic spectra. Hence, transport is governed by two types of chiral quasiparticles: monolayer-like massless ($l = 1$) and bilayer-like massive ($l = 2$) quasiparticles, albeit with a larger effective mass than in a bilayer, $m_{ABA} = \sqrt{2}m_{AB} \approx 0.05m_e$ ($m_{AB} = \gamma_1/(2v^2) \approx 0.035m_e$, where m_e is the electron mass)^{5,6,9}. Recent experiments revealed that in contrast to a bilayer, where application of an electric field across the layers opens a bandgap in the spectrum²⁰, in the ABA trilayer it actually leads to a tunable band overlap^{13–18}.

Although to our knowledge no magnetotransport experiments on ABC trilayers have been published, this case is actually most interesting, as it is expected to present new, $l = 3$ chiral quasiparticles with cubic dispersion^{4–6,10–12}, $\varepsilon(p) = \gamma_1(vp/\gamma_1)$ (ref. 3), see Fig. 1b. That this situation is remarkable could already be seen from the fact that the effective mass of such charge carriers is energy-dependent and diverges at the charge neutrality point (CNP), $m_{ABC} = p(\partial\varepsilon/\partial p)^{-1} = \gamma_1^2/3pv^3 = (2/3)m_{AB}(\gamma_1/\varepsilon)^{1/3}$. This corresponds to a diverging low-energy density of states, $D(\varepsilon) \sim \varepsilon^{-1/3}$, in contrast to a constant $D(\varepsilon)$ in bilayers and a vanishing one in monolayers. Such an abundance of low- ε scattering states would make non-chiral fermions with cubic dispersion unstable with respect to decays—but in ABC trilayers $l = 3$ quasiparticles are protected

¹CMP& MS Department, Brookhaven National Laboratory, Upton, New York 11973, USA, ²Department of Physics, Renmin University of China, Beijing 100872, China, ³Department of Physics and Astronomy, SUNY, Stony Brook, New York 11794, USA, ⁴Department of Physics and Astronomy, University of Iowa, Iowa City, Iowa 52242, USA. *e-mail: zaliznyak@bnl.gov.

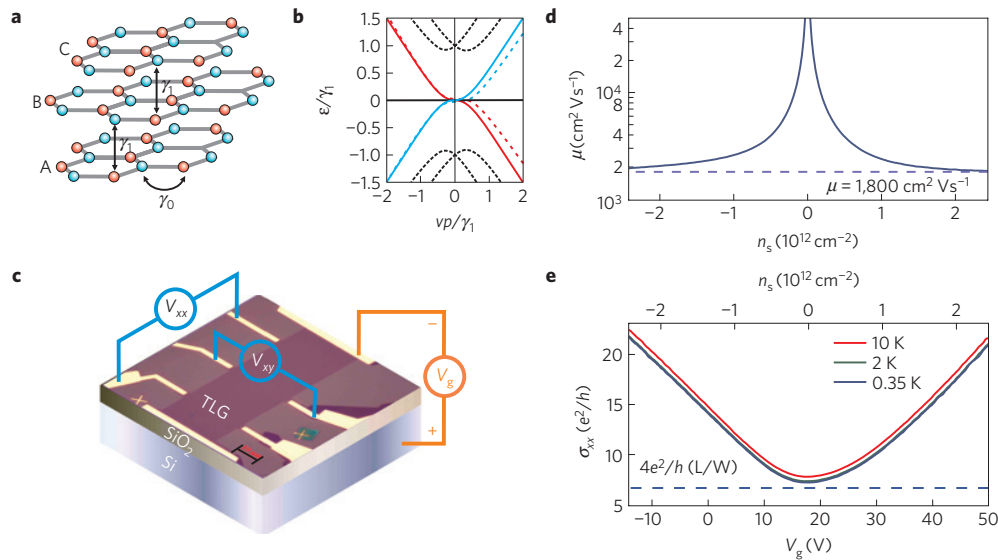


Figure 1 | Mobility and conductance of ABC trilayer graphene. **a**, The structure and, **b**, the low-energy band structure, of ABC-stacked trilayer graphene (ref. 10). **c**, The image of our large-area etched Hall bar, and schematics of the measurement set-up. The black scale bar is 10 μm . **d**, Field mobility, $\mu = \sigma_{xx}/(n_s e)$, and **e**, longitudinal conductivity, as a function of back-gate voltage V_g , or carrier density induced by electric field effect, $n_s = C_g V_g$ (top scale). The minimum conductivity is slightly larger than $\approx 6.7e^2/h$, expected for the ballistic conductance via four quantum channels (dashed line).

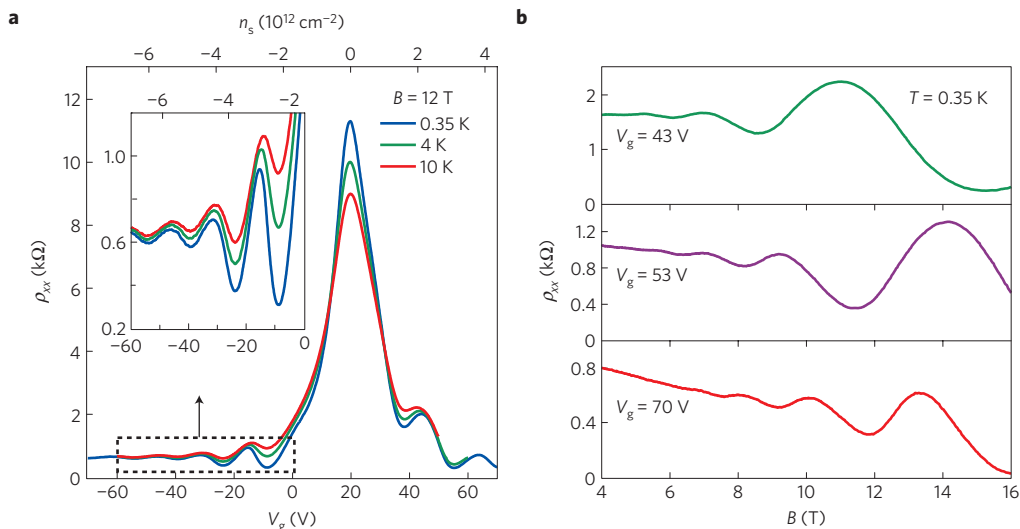


Figure 2 | Temperature and gate voltage dependence of quantum Shubnikov-de Haas Oscillations (SdHO). **a**, Longitudinal resistivity, ρ_{xx} , in magnetic field $B = 12$ T at 0.35 K, 4 K, and 10 K, as a function of V_g (carrier density, top scale). The inset is a zoom-in of the part surrounded by the dashed line. **b**, SdHO as a function of magnetic field for different carrier densities (back-gate voltages). The decay of the SdHO magnitude with temperature and magnetic field is governed by the cyclotron mass of charge carriers, $m_c(n_s)$, and by the quantum scattering time, τ_q .

by chirality conservation. On the other hand, the diverging $D(\epsilon)$ leads to super-polarizability and super-linear screening, which were predicted theoretically in perpendicular electric fields^{11,12}. Although at very low energies cubic dispersion is further modified by long-range hoppings, estimates¹² show that it is valid for carrier densities $n > 10^{11} \text{ cm}^{-2}$, which are of interest for experiments. Also, in SiO_2 -supported samples this fine structure is smeared out by the disorder potential of Coulomb impurities present in the substrate.

Here we report measurements of magnetotransport oscillations and the quantum Hall effect in ABC-stacked trilayer graphene. The optical image of our Hall bar device and schematics of the measurement set-up are shown in Fig. 1c. Our sample was prepared following a standard procedure²¹ by mechanical exfoliation of kish graphite (see Methods). Although the number of layers can already be identified by optical contrast, it was also confirmed

using Raman microspectroscopy, by measuring the full-width at half-maximum (FWHM) of the 2D Raman band^{22,23}. The characteristic asymmetrical shape of the 2D band spectrum, with a dip near $2,700 \text{ cm}^{-1}$, was used to identify the ABC stacking in our sample^{24,25} (see Supplementary Information).

The transport properties of the ABC trilayer seem enigmatic: a naïve estimate of the impurity-limited mobility, following similar arguments to the monolayer case, gives an energy (charge density)-dependent mobility, $\mu \sim \epsilon^{2/3} \sim n_s$ (Supplementary Information). This clearly disagrees with our transport measurements of the ABC trilayer device of Fig. 1c, shown in Fig. 1d,e. We find that the gate voltage dependence of longitudinal conductivity, σ_{xx} , is very similar to that of monolayer/bilayer graphene, with roughly linear asymptotic behaviour at high charge-carrier densities, n_s (or gate voltages V_g), for both polarities (\pm correspond to electrons/holes).

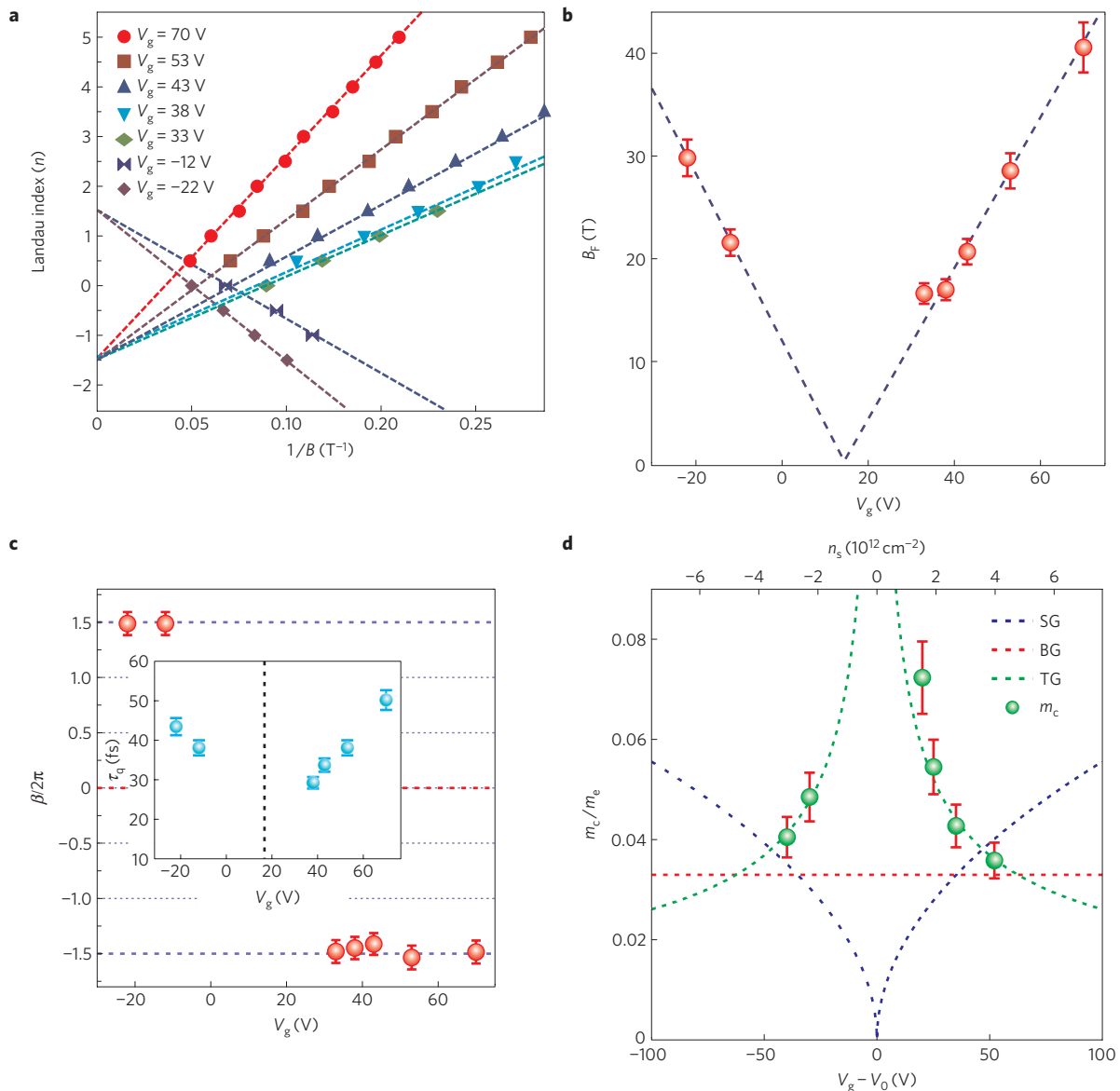


Figure 3 | Berry phase 3π and diverging cyclotron mass in ABC trilayer. **a**, Fan diagram of SdHO. Points for integer n correspond to the n -th minimum, for half-integers, $n-1/2$, to the n -th maximum of $\rho_{xx}(B)$ (refs 1,2). **b**, $B_F(V_g)$ dependence, the error bars show standard deviation, the dashed line is linear fit. **c**, The phase shift of magneto-oscillations from fits in Fig. 3a. The inset shows the quantum scattering time obtained by fitting the SdHO by the ALK formula. **d**, The cyclotron mass, m_c , of charge carriers as a function of $n_s(V_g)$, obtained from the same SdHO-ALK fits. Lines show the semi-classical result for linear (SG), quadratic (BG) and cubic (TG) spectra, with $\gamma_1 = 0.5$ eV obtained by fitting the measured $m_c(n_s)$.

The asymptotic field mobility estimated by assuming a simple Drude model is $\mu = \sigma_{xx}/(en_s) \approx 1,800 \text{ cm}^2 \text{ V}^{-1} \text{ s}^{-1}$ (e is an electron charge) in our trilayer, which is lower than in similarly prepared high-quality monolayer samples. The maximum resistance near the CNP ($V_g \approx 17.3$ V) is $R_0 \approx 5.7 \text{ k}\Omega$, which is close to the inverse of quantum conductance via four degenerate channels, $h/(4e^2) \approx 6.5 \text{ k}\Omega$ (Supplementary Information).

The observed monolayer-like ‘normal’ gate voltage dependence of the conductivity can be reconciled with the ‘abnormal’ cubic dispersion of $l = 3$ chiral fermions if one accounts for super-screening of the impurity Coulomb potential by such quasiparticles. Indeed, in the random phase approximation (RPA) treatment, the screened potential is governed by the diverging density of states near $\varepsilon = 0$, rather than by the bare Coulomb interaction. As a result, the divergence in the transport scattering cross-section is cancelled by the vanishing screened potential, and one obtains charge-density-independent mobility in the ABC trilayer, $\mu_3 = 8/(\pi^2 N_i)$. Here N_i is

the concentration of Coulomb impurities, which are mainly located in the SiO_2 substrate. In monolayer graphene, screening is much weaker, and simply amounts to multiplying the Coulomb impurity potential by a number, so it becomes $U(r) = -\hbar v \alpha / r$. Here $\alpha = e^2/(\hbar v \varepsilon)$ is determined by the dielectric constant of the glass substrate and the screening properties (polarizability) of graphene. A RPA calculation²⁶ gives an effective dielectric constant $\varepsilon \approx 6$ and $\alpha \approx 0.36$. The mobility of the monolayer is $\mu_1 = 1/(\alpha^2 \pi^2 N_i)$. Hence, for an equal number of impurities, $\mu_3/\mu_1 = 8\alpha^2$, and the mobility of the $l = 3$ chiral fermions of the ABC trilayer seem similar to that of the massless fermions of the monolayer, although it could be markedly lower if the effective fine-structure constant in graphene, $[e^2/(\hbar v)]_{\text{eff}}$, which governs α , is smaller than its RPA estimate.

Having thus established a qualitative understanding of zero-field transport in our ABC trilayer sample, we proceeded with magnetotransport measurements in a perpendicular field B . Figure 2 shows examples of SdH quantum magneto-oscillations at

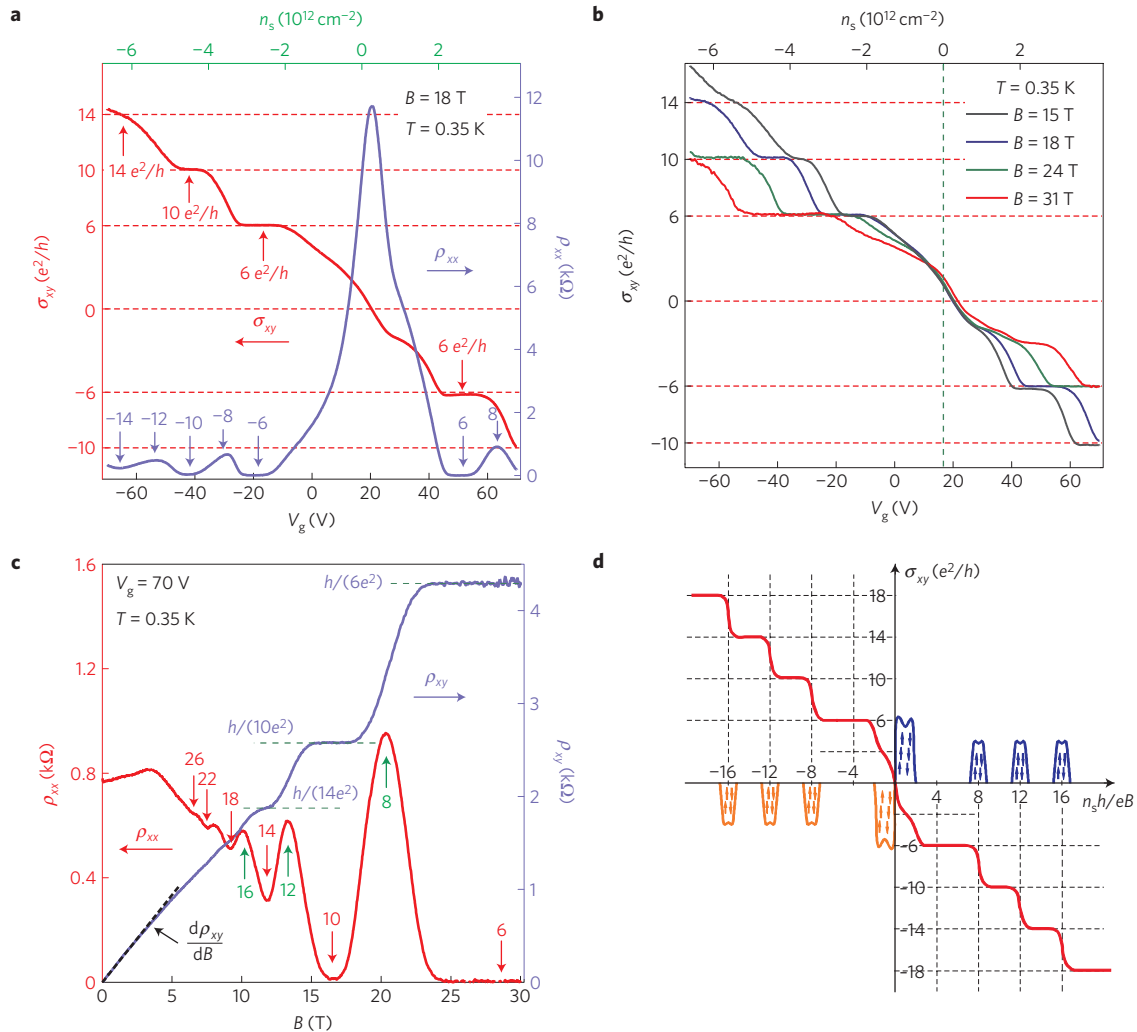


Figure 4 | QHE and Landau Level spectrum in ABC trilayer at $T = 0.35$ K. **a**, Longitudinal resistivity, ρ_{xx} (right scale), and Hall conductivity, $\sigma_{xy} = \rho_{xy} / (\rho_{xx}^2 + \rho_{xy}^2)$ (left scale) at $B = 18$ T. Vertical arrows with numbers show LL filling, $\nu = n_s h / (eB)$, for the corresponding quantum Hall states. **b**, $\sigma_{xy}(V_g)$ for several magnetic fields, B . **c**, ρ_{xx} (left scale), and ρ_{xy} (right scale) as a function of magnetic field for $V_g = 70$ V. Quantized plateaus of ρ_{xy} and zero ρ_{xx} are clearly observed for filling factors $\nu = 6$ and 10 . Dashed horizontal lines show $h/(6e^2)$. Vertical arrows with numbers show LL fillings which can be identified in SdHO. **d**, Schematic illustration of the LL DOS in ABC-stacked trilayer graphene.

temperatures 0.35 K, 4 K and 10 K as a function of gate voltage for $B = 12$ T, and as a function of magnetic field for several V_g . In the semi-classical limit of small oscillations, they can be described by the Ando–Lifshitz–Kosevich (ALK) formula^{27,28}, $(\Delta\rho_{xx}/2\rho_0) = (2\chi/\sinh(\chi))\exp(-\pi/\omega_c\tau_q)\cos((2\pi B_F/B) - \pi + \beta)$. Here, $\chi = 2\pi^2 k_B T / \hbar\omega_c$, k_B is Boltzmann's constant, τ_q is the quantum scattering time, $\omega_c = eB/m_c$ is the cyclotron angular velocity, $m_c = (1/2\pi)(\partial S(\epsilon)/\partial \epsilon) = m_{ABC}$ is the cyclotron mass, $S(\epsilon) = \pi p(\epsilon)^2$ is the area in the momentum space of the orbit at the Fermi energy, $B_F = n_s \Phi_0 / g_{LL}$, where $\Phi_0 = h/e \approx 4.14 \times 10^{-11}$ T cm 2 is the flux quantum and g_{LL} is the LL degeneracy, and $\beta = \pi l$ is the Berry phase of the quasiparticles. Figure 2 already reveals a hallmark of $l = 3$ quasiparticles in the ABC trilayer. The decay of the magnitude of SdH oscillations with increasing temperature, decreasing magnetic field, or increasing charge density n_s , is strikingly fast, much faster than observed in the monolayer or bilayer^{1–3} (at least half a dozen oscillations are seen in similar measurements for the latter systems, whereas we can only reliably identify three to four in Fig. 2).

The simplest analysis of SdH oscillations is achieved by plotting the positions of ρ_{xx} minima and maxima as a function of $1/B$. The Landau fan diagram thus obtained is shown in Fig. 3a. It is already

clear from the linear fits in the figure that charge carriers in our device are characterized by a Berry phase of 3π . Fit parameters are quantified in Fig. 3b,c, which show B_F and β as a function of V_g . Linear fits of $B_F(n_s)$ in Fig. 3b, and using $dn_s/dV_g = 7.59 \times 10^{10}$ cm $^{-2}$ determined from the measured low-field Hall constant, yield the LL degeneracy $g_{LL} = 4 \pm 0.1$, in perfect agreement with the expected valley \times spin degeneracy. Similarly, the average Berry phase in Fig. 3c is $\beta = 2\pi \cdot (1.5 \pm 0.1)$.

We can pursue an analysis of the measured SdHO data further by subtracting the smooth component of magnetoresistance and fitting the oscillating part with the ALK formula (see Supplementary Information). Varying the three parameters, B_F , τ_q , and m_c , we obtain high fidelity fits by imposing a physical constraint, $\tau_q < 200$ fs. The obtained B_F values are within the symbol size of those shown in Fig. 3c. The cyclotron mass of charge carriers obtained by such fitting is shown in Fig. 3d. It shows a marked variation with carrier density, increasing towards the CNP, $n_s = 0$, which is opposite to that observed in monolayer graphene^{1,2}. A fit to the divergent behaviour, $m_c = (\gamma_1^2 / 6\sqrt{\pi} \hbar v^3) n_s^{-1/2}$, expected for $l = 3$ quasiparticles in the ABC trilayer, is shown by the dotted line in Fig. 3d. It yields $\gamma_1 \approx (0.5 \pm 0.1)$ eV (using $v \approx 10^6$ m s $^{-1}$), in good agreement with the γ_1 value expected for few-layer graphene²⁹. This agreement

provides an important credibility check for our analysis, and for τ_q shown in the inset of Fig. 3c. In fact, it is remarkable that we are able to obtain the interlayer hopping parameter from the SdHO data.

Further support for the existence of $l = 3$ charge carriers is provided by the unusual QHE, which develops in our sample at $T \approx 0.35$ K in fields above ≈ 15 T, see Fig. 4. Plateaux of Hall conductivity are observed at $\sigma_{xy} = \pm 6e^2/h, \pm 10e^2/h, \dots$, with a step of $12e^2/h$ between the hole and electron gases across the $N = 0$ LL, confirming its 12-fold degeneracy. This, perhaps, is most clearly seen in Fig. 4c, which shows the magnetic field dependence of the longitudinal, ρ_{xx} , and Hall, ρ_{xy} , resistivities, for $V_g = 70$ V ($n_s \approx 4 \times 10^{12} \text{ cm}^{-2}$). The minima of ρ_{xx} occur near the centre of the ρ_{xy} (σ_{xy}) plateaux, at LL filling factors $\nu = n_s \Phi_0/B = 6, 10, 14, \dots$, as indicated by arrows. The behaviour near the $N = 0$ LL is in stark contrast to that in monolayer and bilayer graphene, where the first QHE plateau develops at $\sigma_{xy} = \pm 2e^2/h$ ($\nu = 2$) and $\sigma_{xy} = \pm 4e^2/h$ ($\nu = 4$), respectively. There is only a weak anomaly in our sample for n_s below the first QHE plateau at $\nu = 6$, which can be associated with $\sigma_{xy} = \pm 3e^2/h$, $\nu = 3$, and is probably an indication of the developing spin- or valley-splitting, or perhaps some other symmetry breaking, see Fig. 4d.

Our results show that new, $l = 3$ chiral fermions indeed exist in ABC trilayer graphene and govern the properties of realistic graphene devices, so they can be detected in experiment. These quasiparticles accumulate a Berry phase of 3π along cyclotron trajectories, acquire unusual LL quantization in magnetic field⁴⁻⁷, $\varepsilon^\pm = \pm(v\hbar\sqrt{2eB}/(\hbar c))^3/\gamma_1^2\sqrt{n(n-1)(n-2)}$, $n = \text{integer}$, and therefore are revealed in magnetotransport measurements, such as we presented here. Not only do our results provide experimental validation for the large body of important recent theoretical work⁴⁻¹², but, perhaps more importantly, they greatly extend the perceived experimental limits, uncovering new and exciting possibilities for future studies. Our findings are also significant because they show the promise of experimentally deploying the unusual properties of the $l = 3$ chiral fermions predicted theoretically¹¹, such as super-screening and bandgap tuning, in realistic graphene devices of practically significant size.

Methods

Our graphene samples were prepared at Brookhaven Center for Functional Nanomaterials. Trilayer flakes for device fabrication were obtained by mechanical exfoliation³⁰ of kish graphite, and deposited onto a 285 nm thick SiO₂ layer thermally grown on a highly doped Si substrate. The number of layers was identified by the optical contrast between graphene and the substrate using optical microscopy with reflected green light, and confirmed using Raman microscopy. Hall bar devices with Cr(3 nm)/Au(30 nm) contacts were patterned and etched using electron-beam lithography and oxygen gas plasma etching.

Four-probe magnetoresistance measurements were performed at the National High Magnetic Field Laboratory, using a low frequency (7 Hz) lock-in technique with a $I = 10$ nA current. Before transfer to the cryostat, devices were annealed for one hour in vacuum at 120 °C to remove impurities. The charge density n_s induced by the gate voltage V_g applied to the Si substrate is determined by the device capacitance, $C_g \approx 121 \text{ aF } \mu\text{m}^2$, which yields $dn_s/dV_g \approx 7.56 \times 10^{10} \text{ cm}^{-2} \text{ V}^{-1}$, in excellent agreement with the low-field Hall constant, giving $dn_s/dV_g \approx 7.59 \times 10^{10} \text{ cm}^{-2} \text{ V}^{-1}$. This agreement indicates that there is little or no charge trapped in the graphene device, and essentially all carriers are doped by the back-gate voltage.

Received 14 June 2011; accepted 22 August 2011; published online 25 September 2011

References

- Novoselov, K. S. *et al.* Two-dimensional gas of massless Dirac fermions in graphene. *Nature* **438**, 197–200 (2005).
- Zhang, Y. B., Tan, Y. W., Stormer, H. L. & Kim, P. Experimental observation of the quantum Hall effect and Berry's phase in graphene. *Nature* **438**, 201–204 (2005).
- Novoselov, K. S. *et al.* Unconventional quantum Hall effect and Berry's phase of 2π in bilayer graphene. *Nature Phys.* **2**, 177–180 (2006).
- Castro Neto, A. H., Guinea, F., Peres, N. M. R., Novoselov, K. S. & Geim, A. K. The electronic properties of graphene. *Rev. Mod. Phys.* **81**, 109–162 (2009).
- Guinea, F., Neto, A. H. C. & Peres, N. M. R. Electronic states and Landau levels in graphene stacks. *Phys. Rev. B* **73**, 245426 (2006).
- Guinea, F., Castro, A. H. & Peres, N. M. R. Electronic properties of stacks of graphene layers. *Solid State Commun.* **143**, 116–122 (2007).
- Aoki, M. & Amawashi, H. Dependence of band structures on stacking and field in layered graphene. *Solid State Commun.* **142**, 123–127 (2007).
- Ezawa, M. Intrinsic Zeeman effect in graphene. *J. Phys. Soc. Jpn* **76**, 094701 (2007).
- Koshino, M. & Ando, T. Orbital diamagnetism in multilayer graphenes: Systematic study with the effective mass approximation. *Phys. Rev. B* **76**, 085425 (2007).
- Koshino, M. & McCann, E. Trigonal warping and Berry's phase $N\pi$ in ABC-stacked multilayer graphene. *Phys. Rev. B* **80**, 165409 (2009).
- Koshino, M. Interlayer screening effect in graphene multilayers with ABA and ABC stacking. *Phys. Rev. B* **81**, 125304 (2010).
- Zhang, F., Bhagawan, S., Min, H. & MacDonald, A. H. Band structure of ABC-stacked graphene trilayers. *Phys. Rev. B* **82**, 035409 (2010).
- Craciun, M. F. *et al.* Trilayer graphene is a semimetal with a gate-tunable band overlap. *Nature Nanotech.* **4**, 383–388 (2009).
- Zhu, W., Neumayer, D., Perebeinos, V. & Avouris, P. Silicon nitride gate dielectrics and band gap engineering in graphene layers. *Nano Lett.* **10**, 3572–3576 (2010).
- Zhu, W., Perebeinos, V., Freitag, M. & Avouris, P. Carrier scattering, mobilities, and electrostatic potential in monolayer, bilayer, and trilayer graphene. *Phys. Rev. B* **80**, 235402 (2009).
- Liu, Y., Goolaup, S., Murapaka, C., Lew, W. S. & Wong, S. K. Effect of magnetic field on the electronic transport in trilayer graphene. *ACS Nano* **4**, 7087–7092 (2010).
- Bao, W. *et al.* Magnetoconductance oscillations and evidence for fractional quantum Hall states in suspended bilayer and trilayer graphene. *Phys. Rev. Lett.* **105**, 246601 (2010).
- Mak, K. F., Shan, J. & Heinz, T. F. Electronic structure of few-layer graphene: Experimental demonstration of strong dependence on stacking sequence. *Phys. Rev. Lett.* **104**, 176404 (2010).
- Freise, E. J. Structure of graphite. *Nature* **193**, 671–672 (1962).
- Zhang, Y. *et al.* Direct observation of a widely tunable bandgap in bilayer graphene. *Nature* **459**, 820–823 (2009).
- Novoselov, K. S. *et al.* Electric field effect in atomically thin carbon films. *Science* **306**, 666–669 (2004).
- Ferrari, A. C. *et al.* Raman spectrum of graphene and graphene layers. *Phys. Rev. Lett.* **97**, 187401 (2006).
- Graf, D. *et al.* Spatially resolved Raman spectroscopy of single- and few-layer graphene. *Nano Lett.* **7**, 238–242 (2007).
- Hao, Y. F. *et al.* Probing layer number and stacking order of few-layer graphene by Raman spectroscopy. *Small* **6**, 195–200 (2010).
- Lui, C. H. *et al.* Imaging stacking order in few-layer graphene. *Nano Lett.* **11**, 164–169 (2011).
- Ando, T. Screening effect and impurity scattering in monolayer graphene. *J. Phys. Soc. Jpn* **75**, 074716 (2006).
- Coleridge, P. T. Small-angle scattering in two-dimensional electron gases. *Phys. Rev. B* **44**, 3793–3801 (1991).
- Coleridge, P. T., Stoner, R. & Fletcher, R. Low-field transport coefficients in GaAs/Ga_{1-x}Al_xAs heterostructures. *Phys. Rev. B* **39**, 1120–1124 (1989).
- Ohta, T. *et al.* Interlayer interaction and electronic screening in multilayer graphene investigated with angle-resolved photoemission spectroscopy. *Phys. Rev. Lett.* **98**, 206802 (2007).
- Novoselov, K. S. *et al.* Two-dimensional atomic crystals. *Proc. Natl Acad. Sci. USA* **102**, 10451–10453 (2005).

Acknowledgements

We acknowledge discussions with E. Mendez, T. Valla, A. Tselik, and D. Kharzeev. Work at BNL was supported by the Materials Sciences and Engineering Division, Office of Basic Energy Sciences, US DOE, under Contract DE-AC02-98CH10886 Y.Z. acknowledges financial support from NSF contract DMR-0705131. Magnetic field experiments were carried out at NHMFL, which is supported by the NSF through DMR-0084173 and by the State of Florida.

Author contributions

I.Z. and L.Z. designed the study; L.Z. fabricated the samples; L.Z. and Y.Z. performed the experiments; I.Z. and L.Z. analysed the data; M.K. provided theoretical estimates; J.C. and L.Z. characterized the samples using Raman spectroscopy; I.Z. and L.Z. wrote the paper and all authors commented on the manuscript.

Additional information

The authors declare no competing financial interests. Supplementary information accompanies this paper on www.nature.com/naturephysics. Reprints and permissions information is available online at <http://www.nature.com/reprints>. Correspondence and requests for materials should be addressed to I.Z.